Journal of Nanobiotechnology

RESEARCH

Open Access

Integrated triple signal amplification strategy for ultrasensitive electrochemical detection of gastric cancer-related microRNA utilizing MoS_2-based nanozyme, hybridization chain reaction, and horseradish peroxidase

Jianfeng Ma[1†], Qunyan Yao[2,3,4†], Suo Lv[1], Jiasheng Yi[1], Dan Zhu[1], Changfeng Zhu[2*], Lianhui Wang[1*] and Shao Su[1*]

Abstract

Early diagnosis and treatment of gastric cancer (GC) play a vital role in improving efficacy, reducing mortality and prolonging patients' lives. Given the importance of early detection of gastric cancer, an electrochemical biosensor was developed for the ultrasensitive detection of miR-19b-3p by integrating MoS_2-based nanozymes, hybridization chain reaction (HCR) with enzyme catalyzed reaction. The as-prepared MoS_2-based nanocomposites were used as substrate materials to construct nanoprobes, which can simultaneously load probe DNA and HCR initiator for signal amplification. Moreover, the MoS_2-based nanocomposites are also employed as nanozymes to amplify electrochemical response. The presence of miR-19b-3p induced the assembly of MoS_2-based nanoprobes on the electrode surface, which can activate in-situ HCR reaction to load a large number of horseradish peroxidase (HRP) for signal amplification. Coupling with the co-catalytic ability of HRP and MoS_2-based nanozymes, the designed electrochemical biosensor can detect as low as 0.7 aM miR-19b-3p. More importantly, this biosensor can efficiently analyze miR-19b-3p in clinical samples from healthy people and gastric cancer patients due to its excellent sensitivity and selectivity, suggesting that this biosensor has a potential application in early diagnosis of disease.

Keywords MoS_2-Au@Pt nanozymes, Electrochemical, Gastric cancer, miRNA, Signal amplification, Clinical samples

†Jianfeng Ma and Qunyan Yao contributed equally to this work.

*Correspondence:
Changfeng Zhu
zhuchangfeng@fudan.edu.cn
Lianhui Wang
iamlhwang@njupt.edu.cn
Shao Su
iamssu@njupt.edu.cn

[1]State Key Laboratory of Organic Electronics and Information Displays & Jiangsu Key Laboratory for Biosensors, Institute of Advanced Materials (IAM), Nanjing University of Posts and Telecommunications, 9 Wenyuan Road, Nanjing 210023, China
[2]Department of Gastroenterology and Hepatology, Zhongshan Hospital, Fudan University, Shanghai 200032, China
[3]Department of Gastroenterology and Hepatology, Zhongshan Hospital (Xiamen), Fudan University, Xiamen 361015, China
[4]Shanghai Geriatric Medical Center, Shanghai 201104, China

Introduction

Gastric cancer is the fifth global incidence rate of malignant tumor, which causes millions new diagnoses and deaths every year [1]. As we know, it is almost no clinical symptoms in the early-stage gastric cancer [2]. Once patients have obvious clinical symptoms, it means that they are in the middle or late stage of gastric cancer [3]. In other word, the 5-year survival rate of those gastric cancer patients is below 20% [4]. Therefore, early diagnosis can efficiently improve the cure rate of gastric cancer and prolong patients' lives. Nowadays, gastroscopy combined with tissue biopsy is considered as the gold standard for detecting gastric cancer [5]. However, it is difficult to use as a routine screening method for gastric cancer due to its invasive nature and high cost. Therefore, it is still a challenge to develop non-invasive, accurate, efficient and fast methods for the early diagnosis of gastric cancer.

Numerous studies have proved that the abnormal expression of microRNA (miRNA) is related with tumorigenesis and tumor progression [6–8]. Moreover, miRNA generally exists in body fluids, such as blood, plasma, and serum in a stable form, which is considered as a promising biomarker for the early diagnosis of different malignant tumors [9]. To date, kinds of miRNAs included miR-21 [10], miR-106b [11], miR-451 [12], miR-486 [13], miR-27a [14] and miR-19b-3p [15] have been identified as potential biomarkers for gastric cancer monitoring and early diagnosis. Among them, miR-19b-3p will downregulated expresses when patients are suffering from gastric-related diseases [15]. More importantly, miR-19b-3p can inhibits the growth, migration, and invasion of gastric cancer cells via negative modulation of neuropilin-1 (NRP1) and epithelial-mesenchymal transition (EMT)/cell adhesion processes [16]. Taken together, miR-19b-3p will be a promising biomarker for early diagnosis of gastric cancer and early cancer screening.

Accurate, fast and selective detection of miRNA is still a challenge due to its features of short length, low abundance and high homology between family members in plasma and serum [17–19]. Traditional detection methods included northern blotting [20], quantitative reverse transcription polymerase chain reaction (qRT-PCR) [21], microarrays [22] and DNA sequencing [23] have their intrinsic drawbacks, such as expensive instruments, complex operations, long analysis time, and professional operators [24]. In view of this, there is an urgent need to develop novel methods featuring the ability to efficiently and conveniently detect miRNA [25, 26].

Herein, an electrochemical biosensor was designed for the ultrasensitive detection of miR-19b-3p by coupling with MoS_2-based nanozymes, hybridization chain reaction (HCR) and enzyme catalyzed reaction. Gold-platinum core-shell nanoparticles-decorated MoS_2 nanocomposites (MoS_2-Au@Pt) with peroxidase-like activity were used to construct nanoprobes for signal amplification [27, 28]. These MoS_2-Au@Pt nanozymes not only can abundantly load capture probes and HCR initiator for improving the efficiency of HCR reaction, but also can catalyze hydrogen peroxide and 3,3',5,5'-tetramethylbenzidine (H_2O_2-TMB) reaction system for signal amplification. In the presence of miR-19b-3p, the assembled MoS_2-based nanoprobes triggered HCR reaction accompanied by a large number of horseradish peroxidase (HRP) immobilized on the electrode surface. The introduced HRP can efficiently catalyze H_2O_2-TMB reaction to generate an outstanding electrochemical signal [25]. Due to the synergistic signal amplification, the proposed electrochemical biosensor can detect as low as 0.7 aM miR-19b-3p. More importantly, this biosensor can efficiently determine miR-19b-3p in clinical samples from healthy people and gastric cancer stage I &III patients due to its excellent sensitivity and selectivity, suggesting that this biosensor has a promising application in early diagnosis of gastric cancer.

Materials and methods

Materials, reagents and apparatus

Materials, reagents, characterization apparatus and electrochemical measurements were listed in Supporting Information.

Clinical blood samples from 8 healthy donors (health) and 16 gastric cancer (GC) patients were collected from Zhongshan Hospital (Shanghai, China), which was approved by the ethics committee of Zhongshan Hospital. The miRcute serum/plasma miRNA isolation kit (Tiangen Biotech Co., Ltd., Beijing, China) was used to extract the total RNA from the clinical blood samples. The processing steps for clinical samples were provided in Supporting Information. All involved nucleic acid sequences were synthesized by Takara Bio. Inc. (China), which are listed in Table S1.

Preparation of MoS_2-based nanoprobe

MoS_2 nanosheets and MoS_2-Au@Pt nanocomposites were synthesized according to our previous works [29]. The detailed prepared process was listed in Supporting Information. After successful synthesis, 1:1 thiol-labelled HCR initiator (HCR-I) and probe DNA (P2) were co-incubated with 90 μL MoS_2-Au@Pt nanocomposites for 12 h at room temperature. Then, the mixture was centrifuged and purified twice to obtain MoS_2-based nanoprobe (P2-HCR-I/MoS_2-Au@Pt) for further use.

Preparation of the electrochemical biosensor

Before the modification, bare gold electrode was pretreated according to the classical cleaning procedure [30]. The polished process was listed in Supporting

Information. After cleaning, the thiol-labelled capture probe 1 (P1) incubated with 10 mM tris(2-carboxyethyl) phosphine (TCEP) in the dark for 1 h to reduce the disulfide bonds. Subsequently, P1 was assembled on the cleaned gold electrode (Au) surface to obtain P1/Au via Au-S bond. After washing, 1 mM MCH was used to block the nonspecific remaining sites of P1/Au for 1 h. Then, 5 μL different concentrations of target miR-19b-3p was incubated on the electrode surface for 1 h. After that, 5 μL P2-HCR-I/MoS_2-Au@Pt nanoprobes were assembled on the electrode after 80 min incubation. Subsequently, the obtained P2-HCR-I/MoS_2-Au@Pt/miR-19b-3p/P1/Au incubated with 5 μL of the mixture hairpin probes (HP1-HP2, 1:1 concentration ratio) at 37 °C for 80 min to accomplish the HCR reaction. Finally, the designed modified electrode was used for electrochemical measurements.

Results and discussions

Design principle of the electrochemical biosensor

As illustrated in Scheme 1, P1 was firstly assembled on electrode surface via Au-S bond. After passivating the electrode surface with MCH, target miR-19b-3p and P2-HCR-I/MoS_2-Au@Pt nanoprobes were introduced to construct P2-HCR-I/MoS_2-Au@Pt/miR-19b-3p/P1/Au due to the formation of P1-miR-19b-3p-P2 sandwiched structure. Then, the assembled HCR-I triggered the occurrence of HCR reaction in the presence of HRP-labelled both HP1 and HP2. As a result, a large number of HRP were assembled on the surface of electrode surface with the occurrence of HCR reaction. Therefore, the assembled MoS_2-Au@Pt nanozymes and HRP can efficiently co-catalyze H_2O_2-TMB reaction to generate outstanding electrochemical signal, achieving the purpose of signal amplification. In this study, a triple signal amplification strategy was designed for miR-19b-3p detection. MoS_2-Au@Pt nanocomposites are not only used as nanoprobes to load P2 and HCR-I for recognizing and capturing miR-19b-3p, but also are employed as nanozymes to catalyze H_2O_2-TMB reaction. At this moment, this biosensor achieved the first signal amplification. In the presence of HP1 and HP2, a typical HCR reaction was initiated by HCR-I. Accompanied by HCR reaction, a super-long DNA double-stranded structure labelled with HRP was obtained on electrode surface, resulting in the second signal amplification. The introduced HRP catalyze H_2O_2-TMB reaction to achieve the third signal amplification. Coupled with the triple signal amplification, this proposed biosensor can qualitatively and quantitatively detect miR-19b-3p with satisfactory results.

Characterization of MoS_2, MoS_2-AuNPs and MoS_2-Au@Pt

Transmission electron microscope (TEM) was used to characterize the morphologies of as-prepared MoS_2, MoS_2-AuNPs and MoS_2-Au@Pt nanomaterials. As shown in Fig. S1, gold nanoparticles (AuNPs) with an average diameter of 8.1±0.7 nm were distributed on the surface of MoS_2 nanosheets, forming MoS_2-AuNPs nanocomposites. Subsequently, MoS_2-AuNPs nanocomposites were used as nanoseeds to prepare MoS_2-Au@

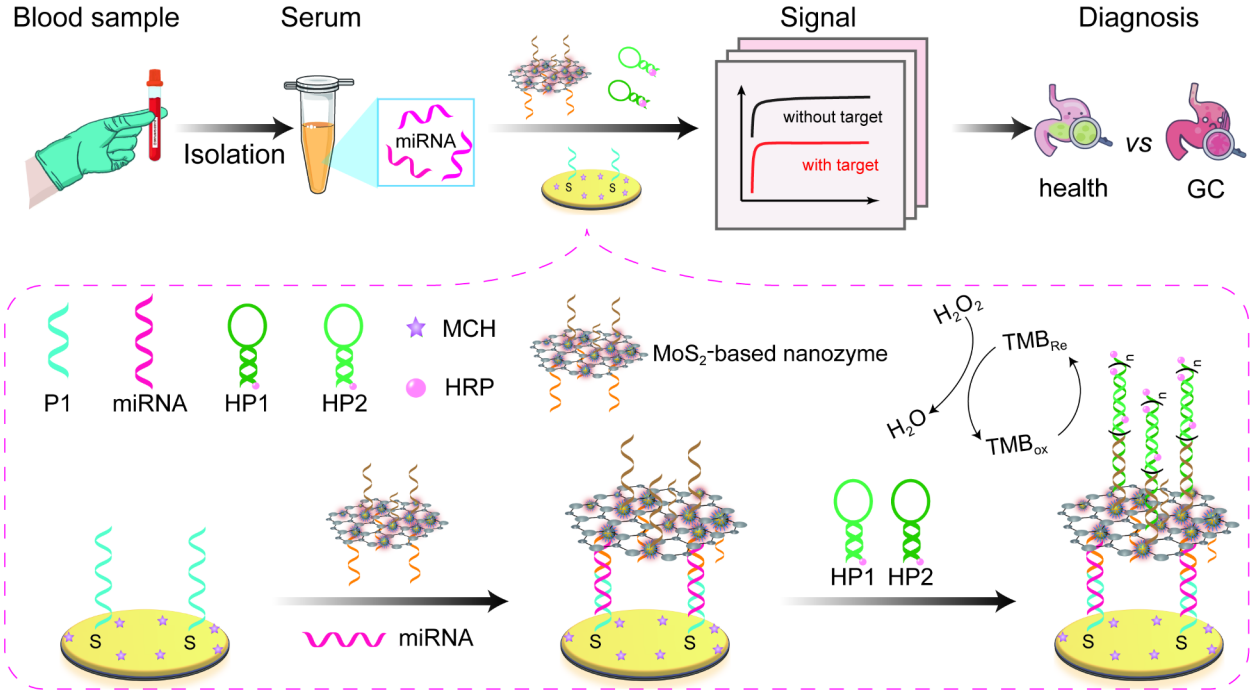

Scheme 1 Schematic illustration of the fabrication process of the electrochemical biosensor for miR-19b-3p detection

Pt nanocomposites. Obviously, 20.1 ± 0.5 nm core-shell Au@Pt bimetallic nanoparticles were supported on MoS_2 surface, proving that the successful synthesis of MoS_2-Au@Pt nanocomposites.

Zeta potential analysis was applied to evaluate the charges of the nanocomposite suspensions. As observed in Fig. S2, the zeta potential of MoS_2 nanosheets was −22.2 mV. Compared with MoS_2 nanosheets, the zeta potential of MoS_2-AuNPs nanocomposites was positively shifted to -13.4 mV, suggesting that the successful decoration of AuNPs [31, 32]. When Au@Pt bimetallic nanoparticles supported on the surface of MoS_2 nanosheets, the zeta potential increased to 11.3 mV, which is ascribed to the positively charged surfactant adsorbed on the nanomaterials surface [33].

Characterization of P2-HCR-I/MoS_2-Au@Pt nanoprobes

Zeta potential was used to verify the preparation of P2-HCR-I/MoS_2-Au@Pt nanoprobes and the occurrence of HCR reaction. As observed in Fig. 1A, the zeta potential of MoS_2-Au@Pt, P2-HCR-I/MoS_2-Au@Pt, HP1/P2-HCR-I/MoS_2-Au@Pt and HP1-HP2/P2-HCR-I/MoS_2-Au@Pt were 11.2 mV, -7.0 mV, -17.0 mV and −25.5 mV, respectively, suggesting that the successful preparation of nanoprobes and the occurrence of HCR reaction on nanocomposites' surface. The reason is ascribed to the negatively charged DNA were assembled on the surface of MoS_2-Au@Pt nanocomposites. The more DNA assembled on nanocomposites' surface, the zeta potential shifted more negatively.

Moreover, the catalytic activities of MoS_2-Au@Pt nanoprobes and nanoprobe-assisted signal amplification system were characterized by using H_2O_2-TMB reaction system (Fig. 1B). No absorption peak of H_2O_2-TMB solution was obtained, suggesting that no catalytic reaction was occurred (curve a). An obvious absorption peak at 652 nm and a blue solution were observed when MoS_2-Au@Pt nanocomposites was added into H_2O_2-TMB solution (Fig. S3). This phenomenon efficiently proves that MoS_2-Au@Pt nanocomposite has a peroxidase-like enzyme activity to catalyze H_2O_2-TMB reaction. Once P2 and HCR-I were co-assembled on the surface of MoS_2-Au@Pt nanocomposites to form P2-HCR-I/MoS_2-Au@Pt nanoprobes, the absorption peak intensity of nanoprobes decreased about 38.3% compared with that of MoS_2-Au@Pt nanocomposites, indicating that P2 and HCR-I partly blocked the catalytic sites of MoS_2-Au@Pt nanocomposites (Fig. S3, curve b in Fig. 1B). To obtain high detection performance, both HP1 and HP2 labelled with HRP were introduced to improve the catalytic ability and accomplish multiple signal amplification. When HP1 was hybridized on the surface of nanoprobes, reaction solution became bluer and the absorption peak intensity increased to 0.7 (curve c). The highest absorption peak intensity (1.0) and the bluest solution colour were observed when both HP1 and HP2 were added into the reaction strategy (curve d), indicating that HCR reaction was successfully occurred on nanocomposites' surface. The largest response was ascribed to the synergistic effect of MoS_2-Au@Pt nanozymes and HRP.

Characterization of preparation process of the electrochemical biosensor

As shown in Fig. 2A, the initiator DNA (HCR-I) can trigger the self-assembly of HP1 and HP2 to generate long DNA double-strands (dsDNA). The HCR product was

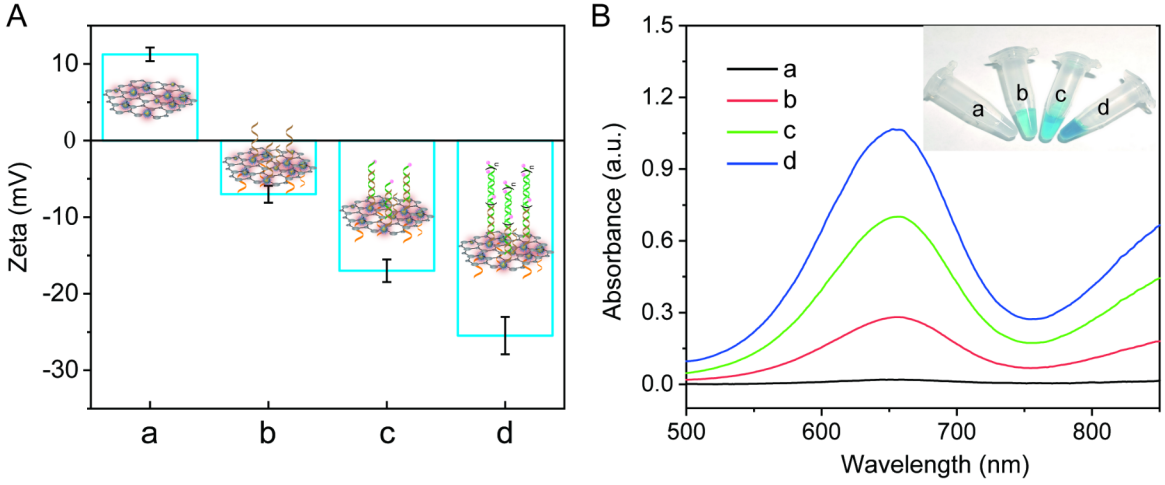

Fig. 1 (**A**) The zeta potentials of (a) MoS_2-Au@Pt, (b) P2-HCR-I/MoS_2-Au@Pt, (c) HP1/P2-HCR-I/MoS_2-Au@Pt and (d) HP1-HP2/P2-HCR-I/MoS_2-Au@Pt. (**B**) UV-visible absorption spectra of (a) H_2O_2-TMB, (b) H_2O_2-TMB + P2-HCR-I/MoS_2-Au@Pt, (c) H_2O_2-TMB + HP1/P2-HCR-I/MoS_2-Au@Pt and (d) H_2O_2-TMB + HP1-HP2/P2-HCR-I/MoS_2-Au@Pt. Inset: the corresponding photograph of different products in H_2O_2-TMB solution

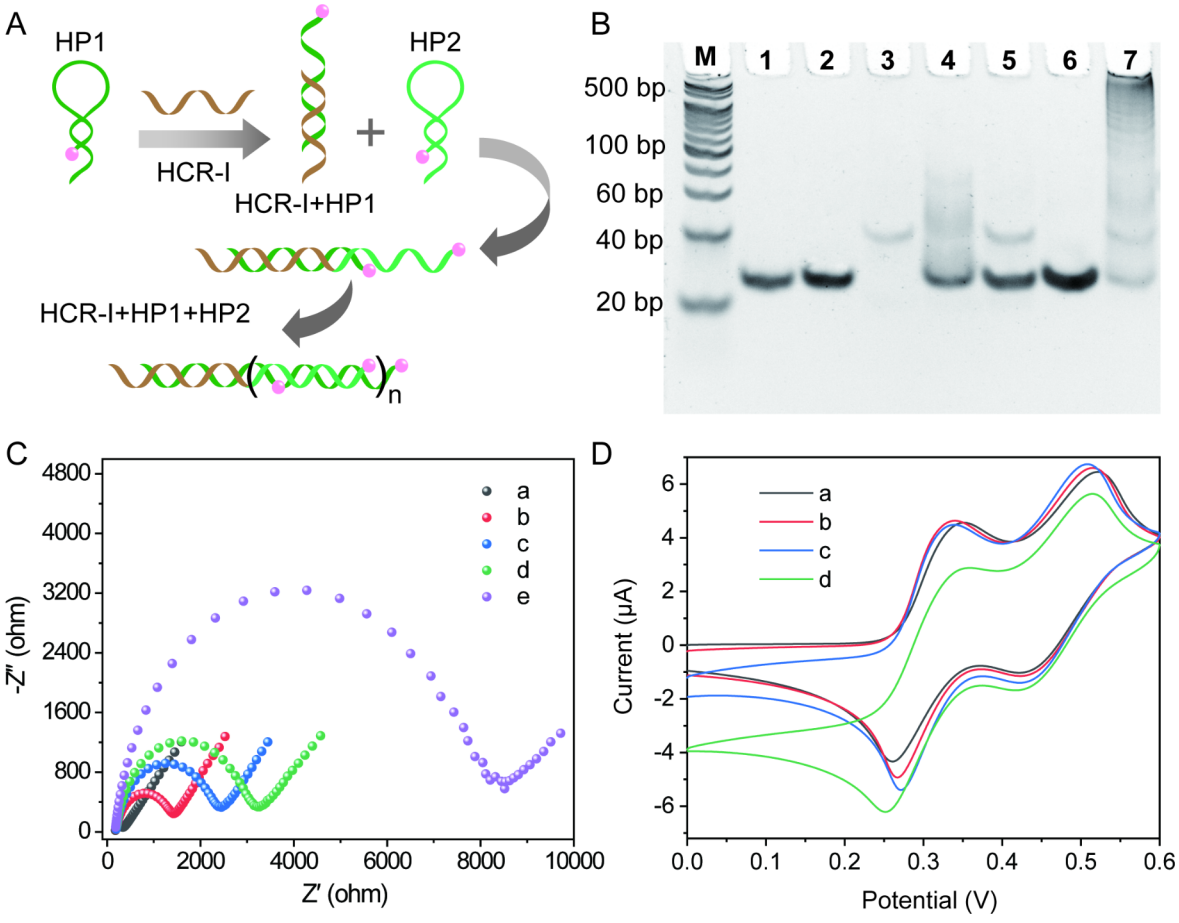

Fig. 2 (**A**) Schematic diagram of HCR process. (**B**) Different products were characterized by gel electrophoresis. From lane M to lane 7 is 20 bp DNA ladder marker, HP1, HP2, HCR-I, HCR-I + HP1, HP2 + HCR-I, HP1 + HP2, HCR-I + HP1 + HP2, respectively. (**C**) EIS curves of (a) bare Au, (b) P1/Au, (c) miR-19b-3p/P1/Au, (d) P2-HCR-I/MoS_2-Au@Pt/miR-19b-3p/P1/Au, (e) HP1-HP2/P2-HCR-I/MoS_2-Au@Pt/miR-19b-3p/P1/Au in 5 mM $K_3[Fe(CN)_6]/K_4[Fe(CN)_6]$ solution containing 0.1 M KCl. (**D**) CV curves of (a) P1/Au, (b) P2-HCR-I/MoS_2-Au@Pt/miR-19b-3p/P1/Au, (c) HP1/P2-HCR-I/MoS_2-Au@Pt/miR-19b-3p/P1/Au, (d) HP1-HP2/P2-HCR-I/MoS_2-Au@Pt/miR-19b-3p/P1/Au in H_2O_2-TMB solution

verified by 8% native polyacrylamide gel electrophoresis (Fig. 2B). Obviously, a single band was observed from lane 1 to lane 3, which is corresponding to HP1, HP2 and HCR-I, respectively. As expectedly, HCR-I can open the hairpin structure of HP1 to form dsDNA structure via hybridization reaction, generating a new band in lane 4. Meanwhile, two bands were obtained in lane 5, suggesting that HCR-I doesn't hybridize with HP2. Moreover, HP1 and HP2 coexist in the reaction system without the trigger of HCR-I (lane 6). In the presence of HCR-I, HCR-I initiates HCR reaction to produce long dsDNA. Correspondingly, ladder bands appeared in lane 7.

Electrochemical impedance spectroscopy (EIS) and cyclic voltammetry (CV) were performed to monitor the fabrication process of this electrochemical biosensor. Generally, the electron transfer resistance (R_{ct}) suggests the interfacial impedance of different modified electrodes. If the negative charges of P1 and miR-19b-3p were assembled on the bare gold electrode surface (curve a, Fig. 2C), the R_{ct} of P1/Au (curve b, Fig. 2C) and miR-19b-3p/P1/Au (curve c, Fig. 2C) increased to 1407.4 Ω and 2426.2 Ω, respectively. With the assembly of P2-HCR-I/MoS_2-Au@Pt nanoprobes, the R_{ct} value was increased to 3207.5 Ω (curve d, Fig. 2C). Once the occurrence of HCR reaction, the introduced HP1 and HP2 caused a great increase in the R_{ct} value of HP1-HP2/P2-HCR-I/MoS_2-Au@Pt/miR-19b-3p/P1/Au (8483.4 Ω, curve e, Fig. 2C). These increase of R_{ct} values proved the successful preparation of the designed electrochemical biosensor. Electrochemical behaviors of different preparation processes were also characterized by CV in $[Fe(CN)_6]^{4-/3-}$solution (Fig. S4). Notably, CV results were in agreement with EIS results, furtherly proving that the designed biosensor have been successfully constructed.

The electrochemical behaviour of this biosensor was also studied in the TMB and H_2O_2 mixture solution. As illustrated in Fig. 2D, two pairs of redox peaks were observed at P1/Au, which was ascribed to the typical

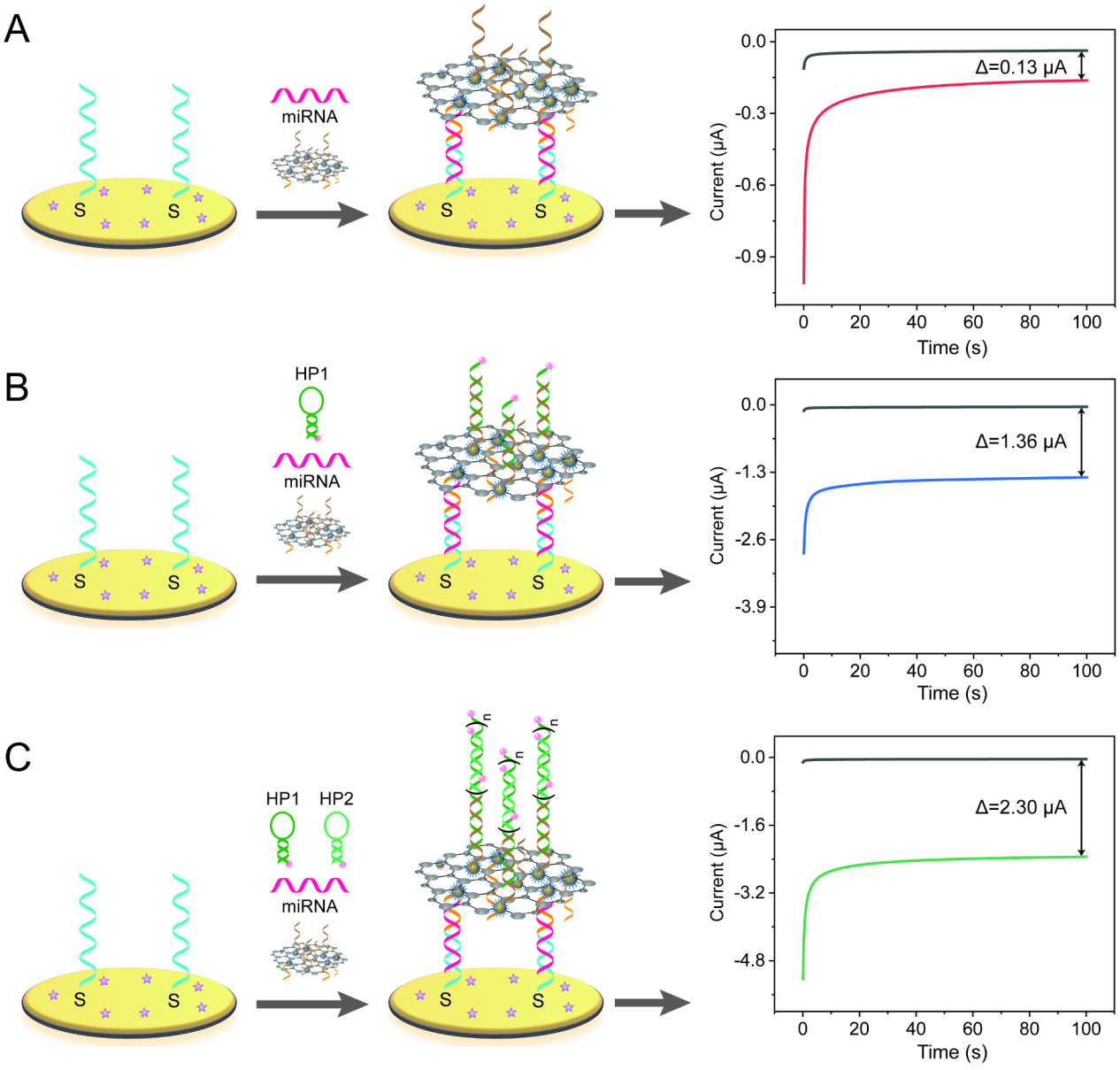

Fig. 3 Electrochemical biosensors with different signal amplification strategies (**A**) single signal amplification (MoS_2-based nanoprobes), (**B**) double signal amplification (MoS_2-based probes + HRP catalytic reaction), (**C**) triple signal amplification (MoS_2-based nanoprobe + HCR reaction + HRP catalytic reaction) for 100 pM miR-19b-3p detection in H_2O_2-TMB solution. The initial potential was 150 mV and the runtime was 100 s

two electron redox reaction of TMB in the presence of H_2O_2 (curve a). After the successful assembly of MoS_2-based nanoprobes, a few increase in the peak current at P2-HCR-I/MoS_2-Au@Pt/miR-19b-3p/P1/Au was observed (curve b). The assembled MoS_2-based nanoprobes have electrocatalytic activity, which can catalyze the reaction of H_2O_2-TMB. When HRP-labelled HP1 and HRP-labelled HP2 were introduced on the electrode surface, an obvious amplified electrochemical responses were obtained at HP1/P2-HCR-I/MoS_2-Au@Pt/miR-19b-3p/P1/Au (curve c) and HP1-HP2/P2-HCR-I/MoS_2-Au@Pt/miR-19b-3p/P1/Au (curve d), respectively. The peak currents were greatly depended on the amount of HRP, which can efficiently catalyze H_2O_2-TMB reaction to generate an outstanding electrochemical signal. All experimental data suggested that the synergistic effect of MoS_2-based nanoprobes, HCR reaction and HRP enzyme can amplify electrochemical signal, which is beneficial for trace target molecules detection.

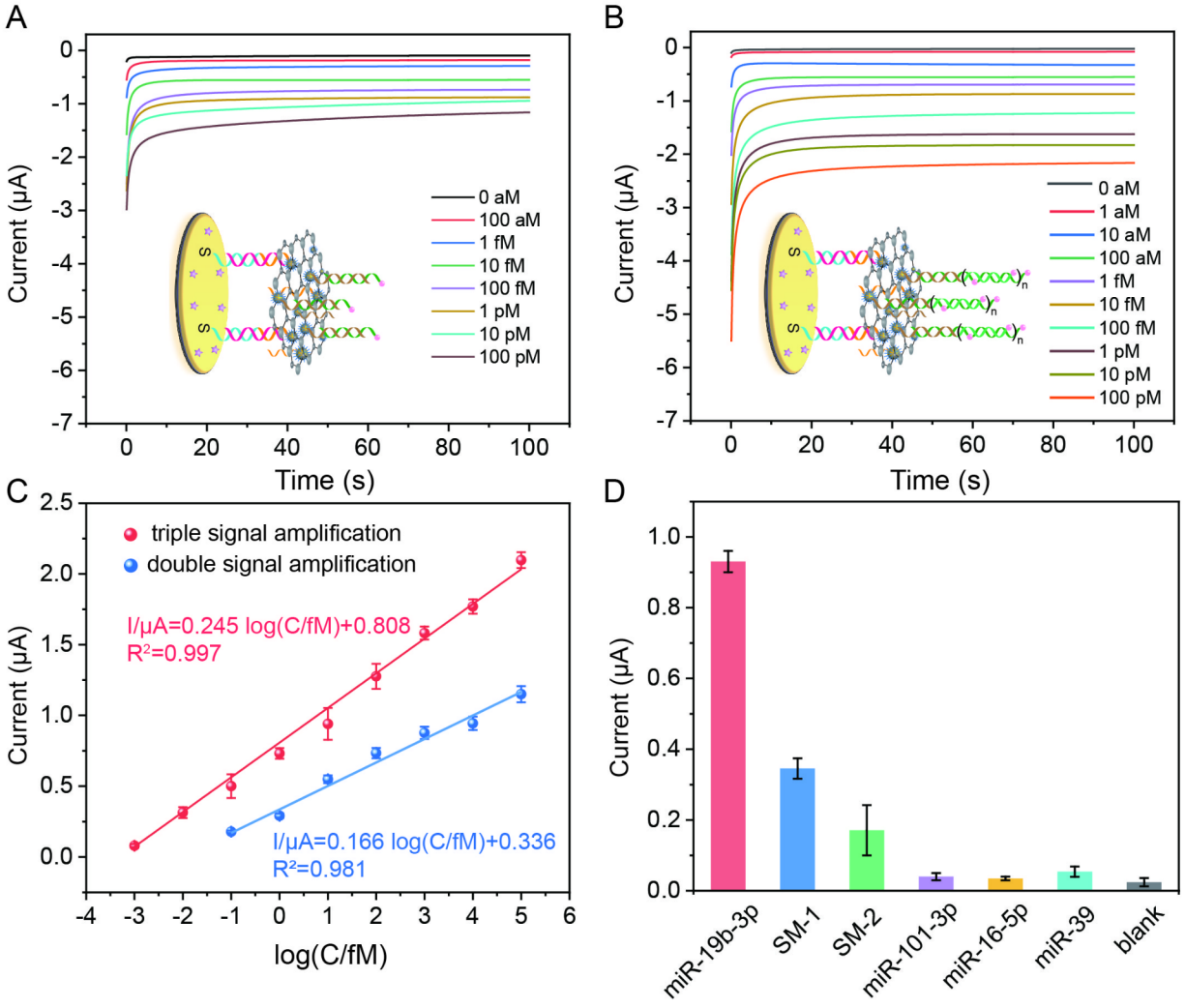

Fig. 4 (**A**) I-t responses of the electrochemical biosensor coupled with double signal amplification strategies for different concentrations of miR-19b-3p detection in H_2O_2-TMB solution. (**B**) I-t responses of the triple signal amplification-based biosensor for different concentrations of miR-19b-3p detection in H_2O_2-TMB solution. The initial potential was 150 mV and the runtime was 100 s. (**C**) The linear relationships between the current value and the logarithm of miR-19b-3p concentrations. (**D**) The selectivity of the biosensor for the detection of 10 fM miR-19b-3p, 10 pM SM-1, 10 pM SM-2, 10 pM miR-101-3p, 10 pM miR-16-5p, and 10 pM miR-39, respectively. The illustrated error bars represent the standard deviations of at least three independent measurements ($n = 3$)

Feasibility of signal amplification strategy

The signal amplification effect of this biosensor was investigated. As mentioned in Scheme 1, MoS_2-based nanozymes, HCR and HRP were used to amplify electrochemical signal. For efficiently realize the signal amplification effect, two control groups included single signal amplification (MoS_2-based nanoprobe) and double signal amplification (MoS_2-based nanoprobe and HRP) were designed for comparison (Fig. 3). For the same concentration of miR-19b-3p detection (100 pM), the peak currents variations ($\Delta I = I_{miRNA} - I_{no\ miRNA}$) of single signal amplification strategy were 0.13 μA (Fig. 3A). By contrast, the ΔI of double signal amplification was reached to 1.36 μA, which is almost 10.46 times than that amplified by single signal amplification (Fig. 3B). For triple signal amplification strategy, the ΔI was about 2.30 μA, which is about 17.69 times and 1.69 times than that of single signal amplification and double signal amplification strategy, respectively, suggesting that the triple signal amplification has the best electrochemical response (Fig. 3C).

Analytical performance of the electrochemical biosensor

To obtain the optimal performance of the electrochemical biosensor, the experimental conditions were optimized. As displayed in Fig. S5A, the optimum incubation time of MoS_2-Au@Pt-based nanoprobes and the reaction time of HCR were selected as 80 min and 80 min, respectively. Under the optimal conditions,

Table 1 Analysis of miR-19b-3p in 1% human serum by using the developed electrochemical biosensor

Samples	Added	Found	RSD (%, $n=3$)	Recovery (%, $n=3$)
1	100 aM	101.70 aM	4.9	101.7
2	1 fM	0.95 fM	5.8	95.2
3	10 fM	9.59 fM	4.6	95.9
4	100 fM	102.50 fM	2.1	102.5
5	1 pM	1.01 pM	3.1	101.1

the analytical performance of electrochemical biosensors coupled with double signal amplification (MoS_2-based nanoprobes+HRP) and triple signal amplification (MoS_2-based nanoprobe+HCR+HRP) for miR-19b-3p detection was tested by using amperometric method, respectively. As shown in Fig. 4A and B, the currents of the biosensors amplified by double signal amplification and triple signal amplification were increasing with the addition of miR-19b-3p, respectively. From the amperometric curves, two linear relationships between the current value at the 100th second and the logarithm of miR-19b-3p concentrations were obtained with equations of $I/\mu\ \mathrm{A} = 0.245\log(C/fM) + 0.808$ (R^2=0.997) and $I/\mu\ \mathrm{A} = 0.166\log(C/fM) + 0.336$ (R^2=0.981) for triple signal amplification- and double signal amplification-based biosensors, respectively (Fig. 4C). Obviously, the triple signal amplification-based biosensor has wider dynamic range (1 aM-100 pM vs. 100 aM-100 pM), larger electrochemical response (0.50 μA vs. 0.18 μA for 100 aM miR-19b-3p detection) and lower detection limit (0.7 aM vs. 37.4 aM) than the double signal amplification-based biosensor. The analytical performance of this triple signal amplification-based biosensor is better than some published works for miRNA detection (Table S2). The selectivity of this triple signal amplification-based biosensor was tested. As shown in Fig. 4D, the current

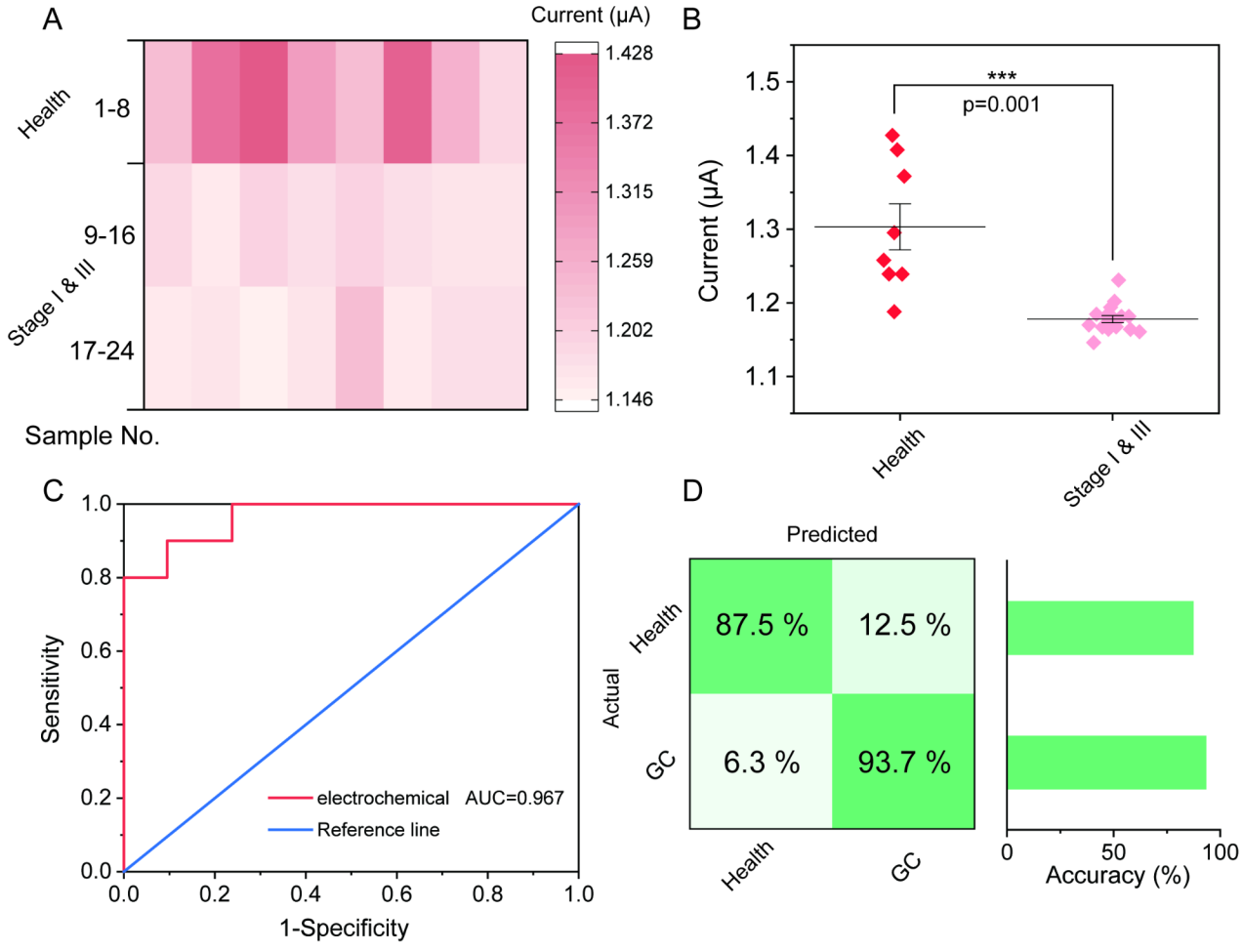

Fig. 5 Analysis of miR-19b-3p expression levels in clinical blood samples by the proposed biosensor. (**A**) Heat map of electrochemical signal of this biosensor for miR-19b-3p detection in the blood of Healthy people, GC stage I & III patients. (**B**) Significant reduction in electrochemical signal for the GC stage I & III patients compared with healthy people ($p=0.001$). (**C**) ROC analysis of miR-19b-3p in clinical blood samples by the electrochemical biosensor. (**D**) Confusion matrix summarizing the GC diagnosis results in a validation cohort

of this biosensor for 10 fM miR-19b-3p detection (0.93 μA) is about 2.7 times, 5.4 times, 23.3 times, 26.6 times, 17.2 times than this biosensor for 10 pM two single-base mismatched miR-19b-3p (SM-1, SM-2), miR-101-3p, miR-16-5p, miR-39 detection, respectively, suggesting that this biosensor can efficiently distinguish target miR-19b-3p from even a single-base mismatched microRNA sequence. The reproducibility of the biosensor was studied by using ten independent biosensors. As shown in Fig. S6, the relative standard deviation (RSD) of intra- and inter-assays were 3.89% and 1.70%, respectively, suggesting that the biosensor has good reproducibility. The storage stability of this biosensor was studied by storing the developed electrodes at 4 °C in the refrigerator. Experimental results showed that the response current of this biosensor was about 92.8% of the initial signal response after 8 days storage, indicating that the biosensor has excellent stability (Fig. S7).

Analysis of miR-19b-3p in clinical samples

At first, simulated serum sample was used to evaluate the practical analytical ability of this biosensor. Typically, different concentrations (100 aM, 1 fM, 10 fM, 100 fM and 1 pM) of miR-19b-3p were added in 1% human serum to simulate the real samples. As displayed in Table 1, the recoveries and relative standard deviation (RSD) of this biosensor are about 95.2-102.5% and 2.1-5.8%, respectively, proving that the proposed biosensor has a promising application in clinical detection.

Based on simulated results, clinical samples were collected to further evaluate the practical application of the electrochemical biosensor. Human serum samples from 16 GC patients at stages I & III and 8 negative control samples were collected and extracted as clinical samples. The concentrations of miR-19b-3p in the clinical samples were determined both by classical qRT-PCR and this biosensor (Table S3). The results in Fig. 5A and Fig. S8 clearly show that the expression level of miR-19b-3p in GC stage I & III patients is lower than that in healthy individuals (Health), indicating that miR-19b-3p is downregulated in GC patients [15, 16, 34, 35]. According to the significant analysis result, the proposed electrochemical biosensor can efficiently distinguish gastric cancer (GC) patients and healthy individuals (Fig. 5B). This conclusion is good agreement with qRT-PCR results, which are recorded in Fig. S9. Moreover, the detection efficacy was also investigated by using a receiver operating characteristic (ROC) curve (Fig. 5C). Notably, the area under the curve (AUC) of this electrochemical biosensor is 0.967. Further analysis showed that the false positive rate was 6.3% and the false negative rate was 12.5%, proving that the accuracies for classification of Health versus GC. (Fig. 5D). Above results further suggested that the proposed electrochemical sensing strategy holds a great potential application in the clinical diagnosis of gastric cancer.

Conclusions

In summary, a triple signal amplification-based electrochemical biosensor was developed for ultrasensitive detection of downregulation miR-19b-3p by coupling with MoS_2-based nanoprobes, enzyme catalysis, and HCR reaction. It is noted that MoS_2-Au@Pt nanomaterials are not only act as substrates to construct nanoprobes for signal amplification, but also used as nanozymes to further amplify electrochemical signal. Due to their outstanding synergistic effect, this designed biosensor exhibited ultrawide dynamic range (1 aM-100 pM) and ultralow detection limit (0.7 aM) for miR-19b-3p detection with excellent selectivity. Moreover, the proposed electrochemical biosensor can accurately quantify miR-19b-3p in clinical blood samples and efficiently distinguish GC patients from healthy individuals, proving that this biosensor is a powerful tool in the early diagnosis of diseases.

Supplementary Information

The online version contains supplementary material available at https://doi.org/10.1186/s12951-024-02848-z.

Supplementary Material 1

Acknowledgements

This work is supported by the Leading-edge Technology Program of Jiangsu Natural Science Foundation (BK20212012), the "Belt and Road" Innovation Cooperation Project of Jiangsu (BZ2022011), the National Natural Science Foundation of China (22274029), the Science and Technology Commission of Shanghai Municipality (22ZR1412000, 22140900700 and 23ZR1411300) and Postgraduate Research & Practice Innovation Program of Jiangsu Province (KYCX22_1011 and SJCX22_0252).

Author contributions

JM: conceptualization, formal analysis, investigation, writing-original draft preparation. QY: formal analysis, data curation, writing-original draft preparation. SL: investigation, data curation. JY: investigation, data curation. DZ: formal analysis, writing-review and editing. CZ: conceptualization, supervision, funding acquisition. LW: supervision, project administration, funding acquisition. SS: conceptualization, writing-review and editing, supervision, project administration.

Data availability

No datasets were generated or analysed during the current study.

Declarations

Ethics approval and consent to participate

This study has been approved by the ethics committee of Zhongshan Hospital and conducted in accordance with ethical guidelines.

Consent for publication

All authors have provided consent for the manuscript to be published.

Competing interests

The authors declare no competing interests.

Received: 19 April 2024 / Accepted: 7 September 2024
Published online: 01 October 2024

References

1. Smyth EC, Nilsson M, Grabsch HI, van Grieken NCT, Lordick F. Gastric cancer. Lancet. 2020;396:635–48.
2. Li B, Zhang F, Niu Q, Liu J, Yu Y, Wang P, Zhang S, Zhang H, Wang Z. A molecular classification of gastric cancer associated with distinct clinical outcomes and validated by an XGBoost-based prediction model. Mol Ther-Nucl Acids. 2023;31:224–40.
3. Van Cutsem E, Sagaert X, Topal B, Haustermans K, Prenen H. Gastric cancer. Lancet. 2016;388:2654–64.
4. Hartgrink HH, Jansen EPM, van Grieken NCT, van de Velde CJH. Gastric cancer. Lancet. 2009;374:477–90.
5. Izumi D, Gao F, Chen Y, Ishimoto T, Horino K, Shimada S, Kodera Y, Baba H, Chen J, Wang X, Goel A. Identification, development and validation of a circulating miRNA-based diagnostic signature for early detection of gastric cancer. Ann Oncol. 2019;30:49.
6. Mitchell PS, Parkin RK, Kroh EM, Fritz BR, Wyman SK, Pogosova-Agadjanyan EL, Peterson A, Noteboom J, O'Briant KC, Allen A, Lin DW, Urban N, Drescher CW, Knudsen BS, Stirewalt DL, Gentleman R, Vessella RL, Nelson PS, Martin DB, Tewari M. Circulating microRNAs as stable blood-based markers for cancer detection. P Natl Acad Sci. 2008;105:10513–8.
7. Ma Y, Tao H. Microribonucleic acids and gastric cancer. Cancer Sci. 2012;103:620–5.
8. Jarry J, Schadendorf D, Greenwood C, Spatz A, van Kempen LC. The validity of circulating microRNAs in oncology: five years of challenges and contradictions. Mol Oncol. 2014;8:819–29.
9. Ouyang T, Liu Z, Han Z, Ge Q. MicroRNA detection specificity: recent advances and future perspective. Anal Chem. 2019;91:3179–86.
10. Li B, Liu F, Peng Y, Zhou Y, Fan W, Yin H, Ai S, Zhang X. Two-stage cyclic enzymatic amplification method for ultrasensitive electrochemical assay of microRNA-21 in the blood serum of gastric cancer patients. Biosens Bioelectron. 2016;79:307–12.
11. Tsujiura M, Ichikawa D, Komatsu S, Shiozaki A, Takeshita H, Kosuga T, Konishi H, Morimura R, Deguchi K, Fujiwara H, Okamoto K, Otsuji E. Circulating microRNAs in plasma of patients with gastric cancers. Br J Cancer. 2010;102:1174–9.
12. Konishi H, Ichikawa D, Komatsu S, Shiozaki A, Tsujiura M, Takeshita H, Morimura R, Nagata H, Arita T, Kawaguchi T, Hirashima S, Fujiwara H, Okamoto K, Otsuji E. Detection of gastric cancer-associated microRNAs on microRNA microarray comparing pre- and post-operative plasma. Br J Cancer. 2012;106:740–7.
13. Oh H-K, Tan AL-K, Das K, Ooi C-H, Deng N-T, Tan IB, Beillard E, Lee J, Ramnarayanan K, Rha S-Y, Palanisamy N, Voorhoeve PM, Tan P. Genomic loss of miR-486 regulates tumor progression and the OLFM4 antiapoptotic factor in gastric cancer. Clin Cancer Res. 2011;17:2657–67.
14. Li Y, Tian Z, Tan Y, Lian G, Chen S, Chen S, Li J, Li X, Huang K, Chen Y. Bmi-1-induced miR-27a and miR-155 promote tumor metastasis and chemoresistance by targeting RKIP in gastric cancer. Mol Cancer. 2020;19:109.
15. Zhang J, Song Y, Zhang C, Zhi X, Fu H, Ma Y, Chen Y, Pan F, Wang K, Ni J, et al. Circulating MiR-16-5p and MiR-19b-3p as two novel potential biomarkers to Indicate Progression of Gastric Cancer. Theranostics. 2015;5:733–45.
16. Wei Y, Guo S, Tang J, Wen J, Wang H, Hu X, Gu Q. MicroRNA-19b-3p suppresses gastric cancer development by negatively regulating neuropilin-1. Cancer Cell Int. 2020;20:193.
17. Jet T, Gines G, Rondelez Y, Taly V. Advances in multiplexed techniques for the detection and quantification of microRNAs. Chem Soc Rev. 2021;50:4141–61.
18. Zhu C, Zhu L, Tan D, Qiu X, Liu C, Xie S, Zhu L. Avenues toward microRNA detection in Vitro: a review of technical advances and challenges. Comput Struct Biotec. 2019;17:904–16.
19. Sun Y, Wang Y, Fang L, Xu T. Signal differentiation models for multiple microRNA detection: a critical review. Anal Bioanal Chem. 2023;415:3967–81.
20. Schwarzkopf M, Pierce NA. Multiplexed miRNA northern blots via hybridization chain reaction. Nucleic Acids Res. 2016;44:e129–129.
21. Fuso P, Di Salvatore M, Santonocito C, Guarino D, Mulè A, Arciuolo D, Mignone F, Rinninella A, Ramundo M, Di Stefano B, Vivolo R, Astone A, Capoluongo ED, Barone C, Cassano A. From PCR to miRNA profiling: where is the true? J Clin Oncol. 2018;36:e12665–12665.
22. Roy S, Soh JH, Ying JY. A microarray platform for detecting disease-specific circulating miRNA in human serum. Biosens Bioelectron. 2016;75:238–46.
23. Androvic P, Benesova S, Rohlova E, Kubista M, Valihrach L. Small RNA-sequencing for analysis of circulating miRNAs: benchmark study. J Mol Diagn. 2022;24:386–94.
24. Valihrach L, Androvic P, Kubista M. Circulating miRNA analysis for cancer diagnostics and therapy. Mol Asp Med. 2020;72:100825.
25. Gao X, Wu H, Li Y, Zhang L, Song M, Fu X, Chen R, Ding S, Zeng J, Li J, Liu P. Dancing in local space: rolling hoop orbital amplification combined with local cascade nanozyme catalytic system to achieve ultra-sensitive detection of exosomal miRNA. J Nanobiotechnol. 2022;20:357.
26. Sun Y, Fang L, Yi Y, Feng A, Zhang K, Xu J-J. Multistage nucleic acid amplification induced nano-aggregation for 3D hotspots-improved SERS detection of circulating miRNAs. J Nanobiotechnol. 2022;20:285.
27. Zhang X, Zhi H, Zhu M, Wang F, Meng H, Feng L. Electrochemical/visual dual-readout aptasensor for Ochratoxin A detection integrated into a miniaturized paper-based analytical device. Biosens Bioelectron. 2021;180:113146.
28. Gong L, Chen B, Tong Y, Luo Y, Zhu D, Chao J, Wang L, Su S. Two-in-one sensing platform for the detection of exosomes based on molybdenum disulfide-based nanozymes. Sens Actuat B-Chem. 2024;398:134686.
29. Dong Y, Wan L, Lv S, Zhu D, Su S, Chao J, Wang L. Construction of a Molybdenum Disulfide-based colorimetric sensor for label-free infectious disease analysis coupled with a Catalyzed Hairpin Assembly reaction. Langmuir. 2022;38:1791–6.
30. Zhang J, Song S, Wang L, Pan D, Fan C. A gold nanoparticle-based chronocoulometric DNA sensor for amplified detection of DNA. Nat Protoc. 2007;2:2888–95.
31. Fang Y, Guo S, Zhu C, Zhai Y, Wang E. Self-assembly of Cationic Polyelectrolyte-Functionalized Graphene nanosheets and Gold nanoparticles: a two-dimensional heterostructure for Hydrogen Peroxide sensing. Langmuir. 2010;26:11277–82.
32. Su S, Sun Q, Wan L, Gu X, Zhu D, Zhou Y, Chao J, Wang L. Ultrasensitive analysis of carcinoembryonic antigen based on MoS_2-based electrochemical immunosensor with triple signal amplification. Biosens Bioelectron. 2019;140:111353.
33. Gupta A, Vasudevan S. Understanding surfactant stabilization of MoS_2 nanosheets in aqueous dispersions from Zeta potential measurements and molecular dynamics simulations. J Phys Chem C. 2018;122:19243–50.
34. Wang N, Wang L, Yang Y, Gong L, Xiao B, Liu X. A serum exosomal microRNA panel as a potential biomarker test for gastric cancer. Biochem Biophys Res Commun. 2017;493:1322–8.
35. Lario S, Quilez ME, Vila-Casadesus M, Aransay AM, González-Lahera A, Lozano J, Macias N, Brunet-Vega A, Lavin JL, Pericay C, Garcia-Martinez L, Montserrat A, Miquel M, Lázaro MJR, Calvet X. The expression of mir-19b-3p and HIPK3 is highly correlated in patients with precancerous lesions of gastric cancer. Gastroenterology. 2017;152:S664–5.

Publisher's note